Electronic Supplementary Material (ESI) for Nanoscale.

Supporting Information

MOF-derived CoNi,CoO,NiO@N–C Bifunctional Oxygen Electrocatalysts for Liquid and All-Solid-State Zn–Air Batteries

Xinde Duan[1], Shuangshuang Ren[1], Fayuan Ge[1], Xukun Zhu[2], Mingdao Zhang[2] and Hegen Zheng[1*]

[1]State Key Laboratory of Coordination Chemistry, School of Chemistry and Chemical Engineering, Collaborative Innovation Center of Advanced Microstructures, Nanjing University, Nanjing 210023, PR China

[2]School of Environmental Science and Engineering, Nanjing University of Information Science & Technology, Jiangsu Key Laboratory of Atmospheric Environment Monitoring and Pollution Control, Collaborative Innovation Center of Atmospheric Environment and Equipment Technology, Nanjing 210044, PR China

* Corresponding author

E-mail: zhenghg@nju.edu.cn

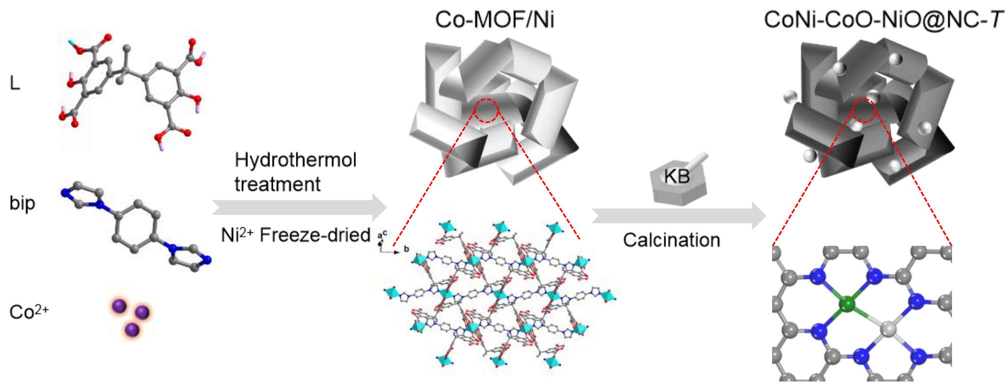

Figure S1. A schematic illustration for the synthesis of hierarchically porous CoNi-CoO-NiO@NC-T.

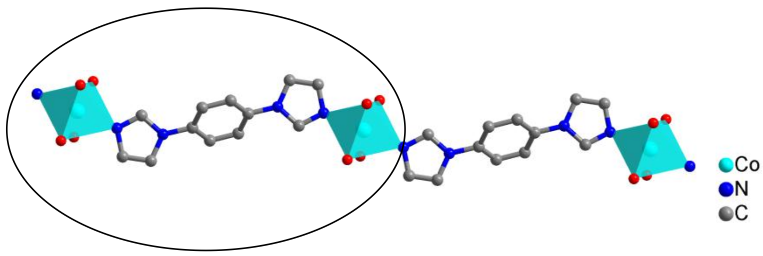

Figure S2. Coordination mode of 1,4-di(1H-imidazol-1-yl)benzene in Co-MOF.

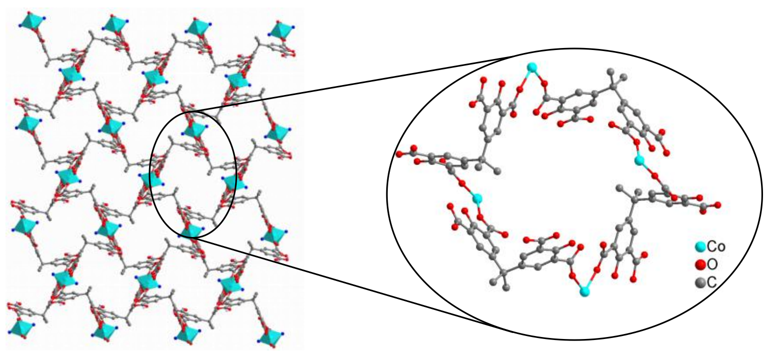

Figure S3. The 48-membered ring formed by four nearby H_6L molecules coordinating to metal atoms in Co-MOF.

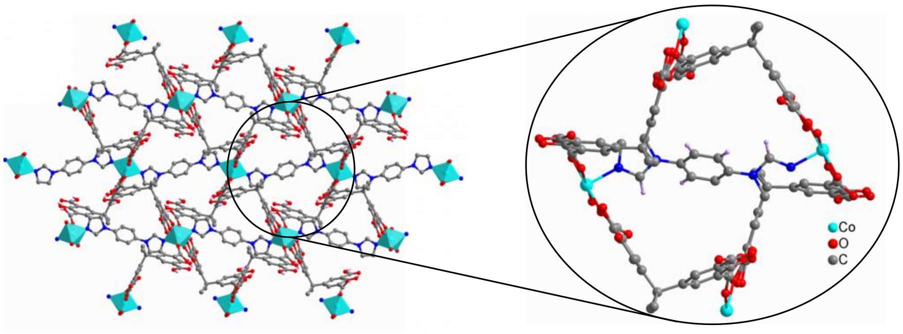

Figure S4. View of 2D architecture of Co-MOF.

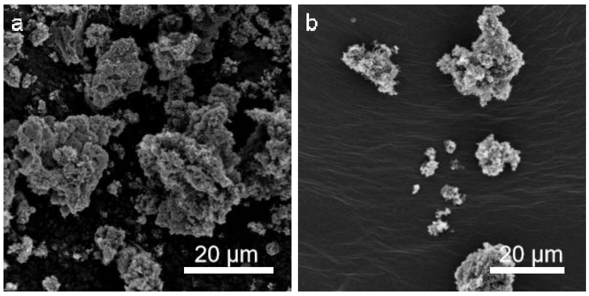

Figure S5. SEM images of CoNi-CoO-NiO@NC-700 (a) and CoNi-CoO-NiO@NC-900 (b).

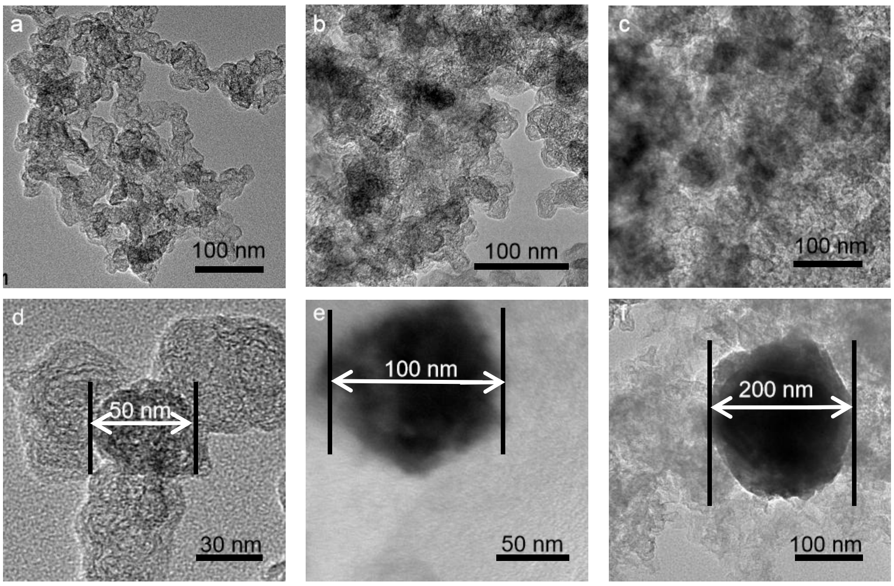

Figure S6. TEM images of CoNi-CoO-NiO@NC-700 (a, d), CoNi-CoO-NiO@NC-800 (b, e), CoNi-CoO-NiO@NC-900 (c, f) after carbonization.

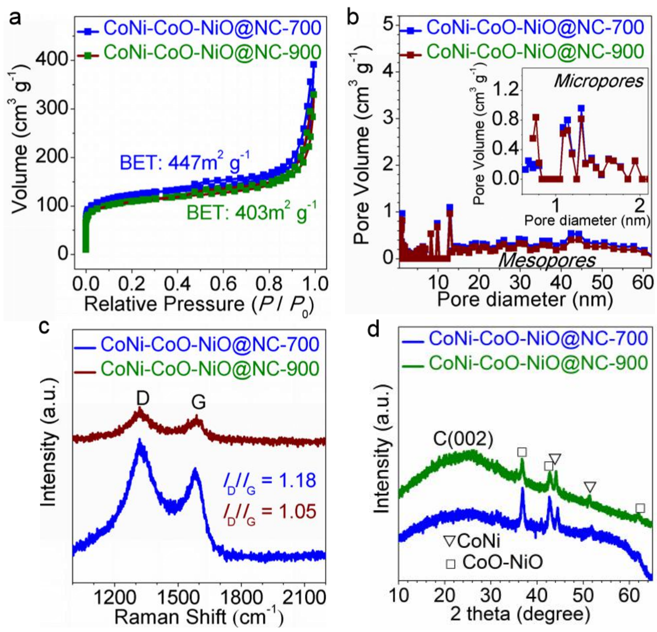

Figure S7. (a) N_2 adsorption-desorption isotherms for CoNi-CoO-NiO@NC-T (700, 900). (b) Related pore size distributions for CoNi-CoO-NiO@NC-T (700, 900). Raman (c) and XRD (d) spectra of CoNi-CoO-NiO@NC-T (700, 900).

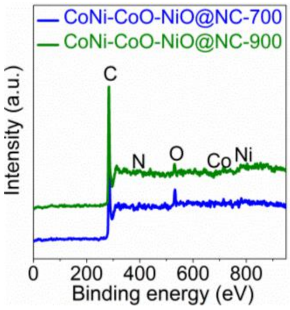

Figure S8. XPS spectra of CoNi-CoO-NiO@NC-T (700, 900).

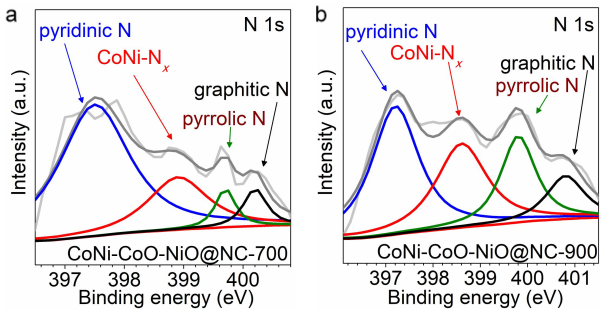

Figure S9. The high resolution N 1s XPS spectra of CoNi-CoO-NiO@NC-700 (a) and CoNi-CoO-NiO@NC-900 (b).

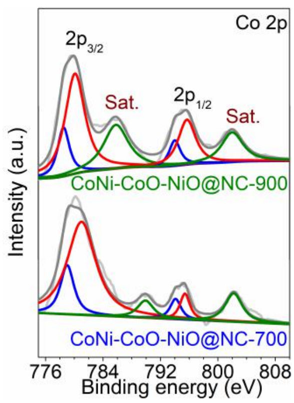

Figure S10. The high resolution Co 2p XPS spectra of CoNi-CoO-NiO@NC-T (700, 900).

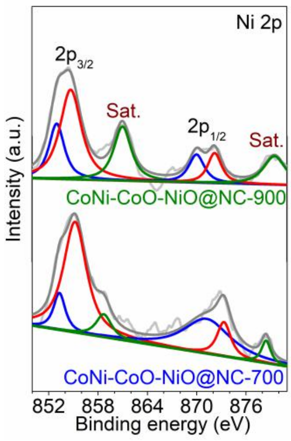

Figure S11. The high resolution Ni 2p XPS spectra of CoNi-CoO-NiO@NC-T (700, 900).

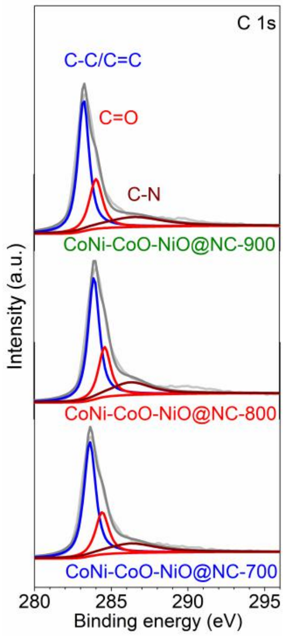

Figure S12. The high resolution C 1s XPS spectra of CoNi-CoO-NiO@NC-T.

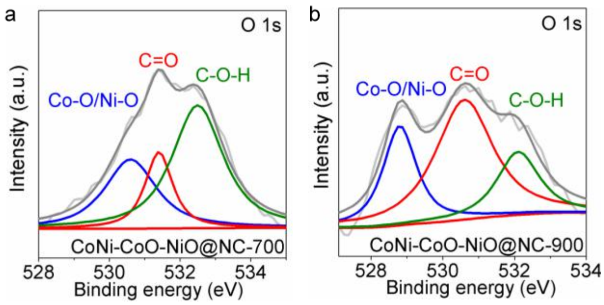

Figure S13. The high resolution O 1s XPS spectra of CoNi-CoO-NiO@NC-700 (a) and CoNi-CoO-NiO@NC-900 (b).

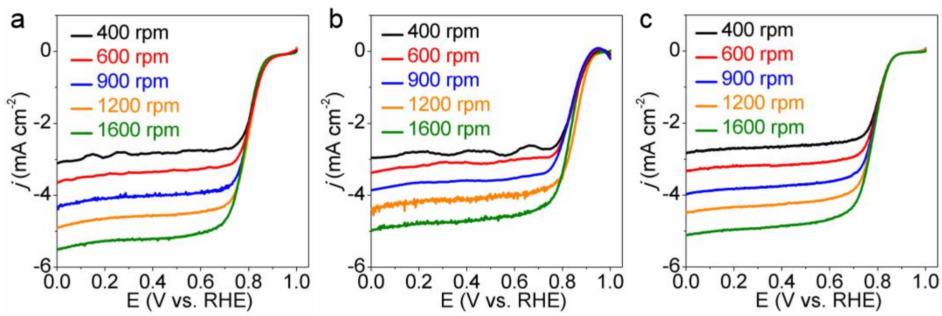

Figure S14. The ORR polarization curves at different rotating rates of CoNi-CoO-NiO@NC-700 (a), CoNi-CoO-NiO@NC-800 (b), and CoNi-CoO-NiO@NC-900 (c).

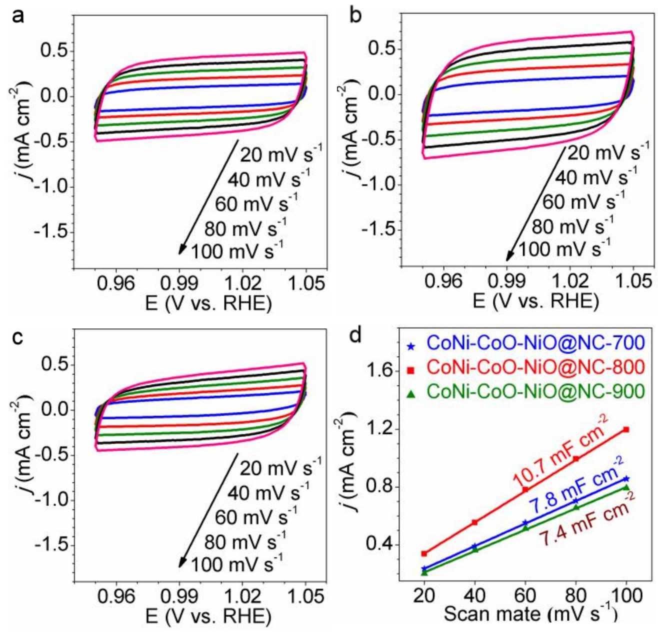

Figure S15. CVs for CoNi-CoO-NiO@NC-700 (a), CoNi-CoO-NiO@NC-800 (b) and CoNi-CoO-NiO@NC-900 (c) in the region of 0.95-1.05 V vs RHE. (d) The C_{dl} measured by taking CV at different scan rates.

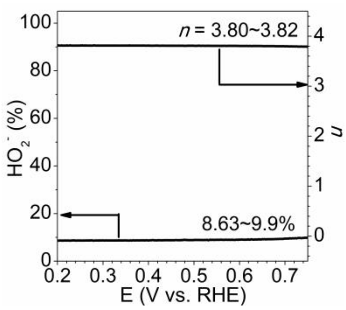

Figure S16. H_2O_2 yield and electron transfer number of CoNi-CoO-NiO@NC-800.

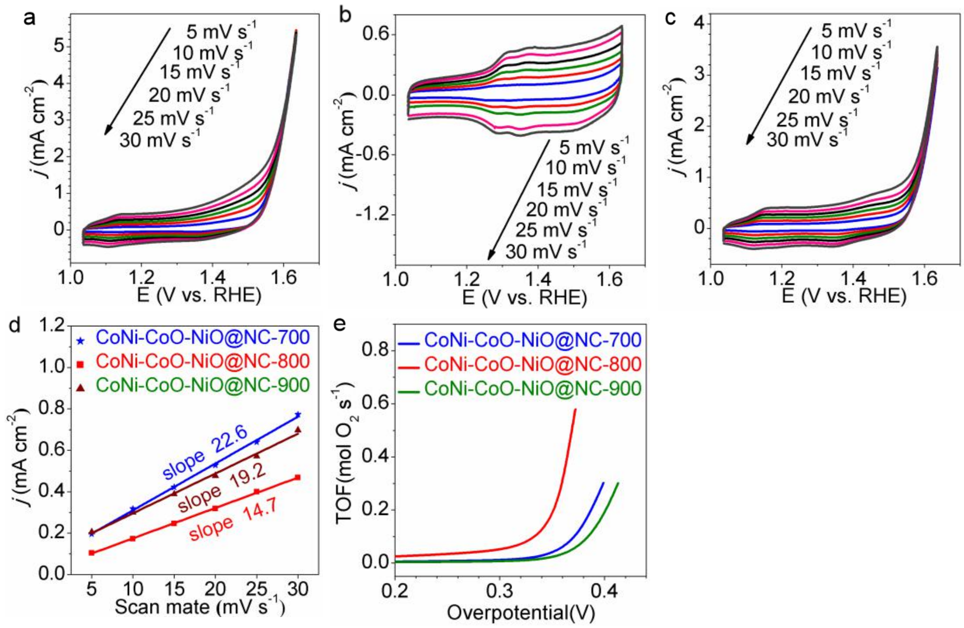

Figure S17. CVs for CoNi-CoO-NiO@NC-700 (a), CoNi-CoO-NiO@NC-800 (b) and CoNi-CoO-NiO@NC-900 (c) in the faradic capacitance current range at scan rates from 5 to 30 mV s^{-1} in 0.1 M KOH. (d) The corresponding plot of oxidation peak current versus the scan rate from CVs. (e) Plot of TOF for CoNi-CoO-NiO@NC-T as a function of overpotential.

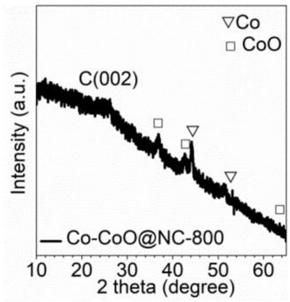

Figure S18. PXRD pattern of Co-CoO@NC-800.

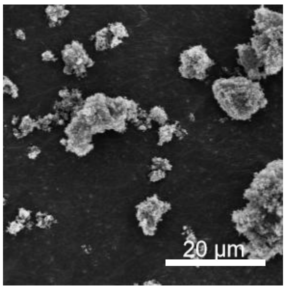

Figure S19. SEM image of Co-CoO@NC-800.

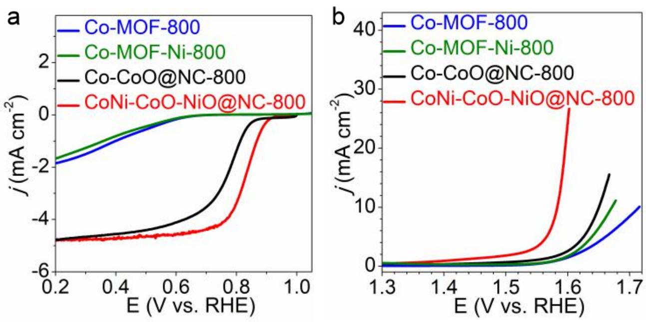

Figure S20. (a, b) LSV curves of samples obtained at an RDE (1600 rpm).

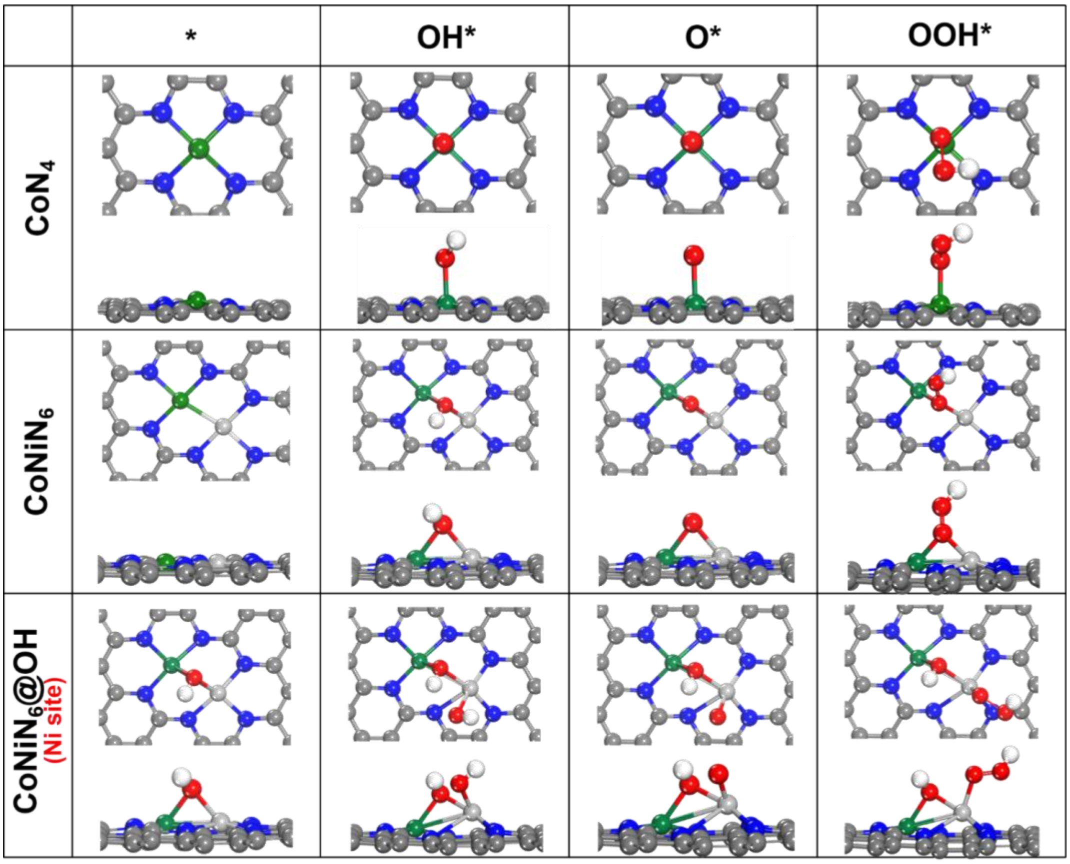

Figure S21. Optimized atomic configurations of oxygen intermediates (OOH*, O*, and OH*) adsorbed on CoN_4, $CoNiN_6$, and $CoNiN_6$@OH (Ni site) models.

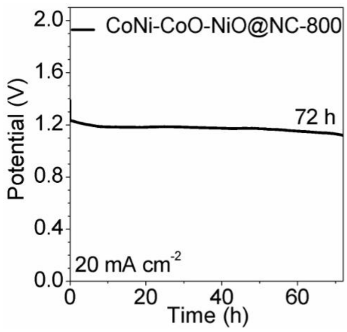

Figure S22. Discharging curves of the primary Zn–air batteries using CoNi-CoO-NiO@NC-800 as ORR catalyst at a current density of 20 mA cm^{-2}.

Table S1. Selected bond lengths (Å) and angles (º) for Co-MOF.

Co-MOF			
Co(1)-N(1)#1	2.0649(15)	Co(1)-N(1)	2.0650(14)
Co(1)-O(1)#1	2.1212(12)	Co(1)-O(1)	2.1212(12)
Co(1)-O(9)#2	2.1341(12)	Co(1)-O(9)#3	2.1341(12)
N(1)#1-Co(1)-N(1)	180.0	N(1)#1-Co(1)-O(1)#1	93.99(5)
N(1)-Co(1)-O(1)#1	86.01(5)	N(1)#1-Co(1)-O(1)	86.01(5)
N(1)-Co(1)-O(1)	93.99(5)	O(1)#1-Co(1)-O(1)	180.0
N(1)#1-Co(1)-O(9)#2	90.30(5)	N(1)-Co(1)-O(9)#2	89.70(5)
O(1)#1-Co(1)-O(9)#2	97.44(5)	O(1)-Co(1)-O(9)#2	82.56(5)
N(1)#1-Co(1)-O(9)#3	89.70(5)	N(1)-Co(1)-O(9)#3	90.30(5)
O(1)#1-Co(1)-O(9)#3	82.56(5)	O(1)-Co(1)-O(9)#3	97.44(5)
O(9)#2-Co(1)-O(9)#3	180.00(6)		

Note：#1 -x+1,-y+1,-z; #2 x-1/2,-y+1/2,z-1/2; #3 -x+3/2,y+1/2,-z+1/2; #4 -x+1,-y+2,-z; #5 -x+3/2,y-1/2,-z+1/2.

Table S2. XPS spectra analysis for CoNi-CoO-NiO@NC-T samples.

Sample	C1s (%)	N1s (%)	O1s (%)	Co2p (%)	Ni2p (%)
CoNi-CoO-NiO@NC-700	90.98	2.61	5.53	0.60	0.28
CoNi-CoO-NiO@NC-800	91.99	2.87	3.38	0.92	0.84
CoNi-CoO-NiO@NC-900	92.4	1.96	4.15	1.02	0.47

Table S3. XPS spectra analysis for CoNi-CoO-NiO@NC-T samples of N 1s signal.

Sample	Pyridinic N	CoNi–N_x	Pyrrolic N	Graphitic N
CoNi-CoO-NiO@NC-700	397.5 eV, 66.0%	398.9 eV, 22.4%	399.7 eV, 5.5%	400.2 eV, 6.1%
CoNi-CoO-NiO@NC-800	398.0 eV, 49.0%	398.9 eV, 35.5%	399.5 eV, 6.4%	400.3 eV, 9.1%
CoNi-CoO-NiO@NC-900	397.2 eV, 40.6%	398.6 eV, 28.6%	399.8 eV, 20.0%	400.8 eV, 10.8%

Table S4. Comparison of bifunctional catalytic performance in alkaline solution between CoNi-CoO-NiO@NC-800 and other previously reported catalysts.

Catalysts	OER performance Overpotential [mV]	ORR performance $E_{1/2}$ [V]	$\triangle E$ [V]	Ref.
CoNi-CoO-NiO@NC-800	**352**	**0.83**	**0.75**	**This work**
Cu@NCNT/Co_xO_y	370	0.82	0.78	[1]
Co@Co_3O_4/NC-2	410	0.74	0.9	[2]
ZnCo-PVP-900	420	0.83	-	[3]
CoDNi-N/C	360	0.81	0.78	[4]
FeCo/NC-800	440	0.8	-	[5]
Fe@N-C	480	0.83	-	[6]
$CuCo_2O_4$/N-CNTs	460	0.79	0.9	[7]
3DOM-Co@TiO_xN_y	385	0.84	-	[8]
Mo-N/C@MoS_2	390	0.81	-	[9]
Co-BTC-bipy-700	400	0.79	0.84	[10]

Table S5. The ΔE_{ads} and ΔG_{ads} of oxygenated intermediates involved in OER/ORR processes on CoN_4, $CoNiN_6$, and $CoNiN_6$@OH.

Intermediates	CoN_4 (eV)	$CoNiN_6$ (eV)	$CoNiN_6$ (eV) (Co site)	$CoNiN_6$ (eV) (Ni site)
ΔE_{OH*}	0.82	-0.05	0.93	0.90
ΔG_{OH*}	0.86	0.23	1.59	1.55
ΔE_{O*}	3.21	0.73	2.75	2.64
ΔG_{O*}	3.16	0.68	2.69	2.59
ΔE_{OOH*}	3.79	3.44	4.06	3.80
ΔG_{OOH*}	3.80	3.65	4.42	4.16

Table S6. The Peak power density of recently reported bifunctional electrocatalysts.

Catalyst	Current density (mA cm^{-2})	Peak power density (mW cm^{-2})	Ref.
CoNi-CoO-NiO@NC-800	**310**	**223**	**This work**
Co_4N/CNW/CC	250	174	[11]
FeNi-NC	115	80.8	[12]
NCNT/CoO-NiO-NiCo	-	102	[13]
S-GNS/$NiCo_2S_4$	-	216	[14]
Co-MOF	150	86.2	[15]
$CuCo_2O_4$/N-CNTs	150	83.8	[7]
NiO/CoN PINWs	200	79.6	[16]
$Fe_{0.5}Ni_{0.5}$@N-GR	150	85	[17]
NCNF-1000	300	185	[18]
Co/CoO@Co-N-C	220	157	[19]

Table S7. The rechargeable ZAB performance of recently reported bifunctional ORR/OER electrocatalysts.

Catalyst	Current density ($mA\ cm^{-2}$)	Number of cycle	Voltage gap increased (V)	Ref.
CoNi-CoO-NiO@NC-800	**2**	**450**	**0.18**	**This work**
NPMC-1000	2	180	0.7	[20]
N-GRW	2	160	0.16	[21]
Fe/N-C	10	100	0.16	[6]
RuO_2-coated MCNAs	2	100	0.1	[22]
Co-N,B-CSs	5	128	1.35	[14]
S,N-Fe/N/C-CNT	5	100	1	[15]
Co_3O_4-NP/N-rGO	5	118	0.87	[7]

Reference

1. X.L. Zhao, F.Li, R.N. Wang, J.M. Seo, H.J. Choi, S.M. Jung, J. Mahmood, I.Y. Jeon and J.B. Baek, *Adv. Funct. Mater.*, 2017, **27**, 1605717.
2. A. Aijaz, J. Masa, C. Rçsler, W. Xia, P. Weide, A.J.R. Botz, R.A. Fischer, W. Schuhmann and M. Muhler, *Angew. Chem. Int. Ed.*, 2016, **55**, 4087-4091.
3. C. Deng, K.H. Wu, J. Scott, S.M. Zhu, X.F. Zheng, R. Amal and D.W. Wang, *ACS Appl. Mater. Interfaces*, 2019, **11**, 9925-9933.
4. Z.H. Li, H.Y. He, H.B. Cao, S.M. Sun, W.L. Diao, D.L. Gao, P.L. Lu, S.S. Zhang, Z. Guo, M.J. Li, R.J. Liu, D.H. Ren, C.M. Liu, Y. Zhang, Z. Yang, J.K. Jiang and G.J. Zhang, *Appl. Catal. B Environ.*, 2019, **240**, 112-121.
5. N. Wu, Y.P. Lei, Q.C. Wang, B. Wang, C. Han and Y.D. Wang, *Nano Res.*, 2017, **10**, 2332-2343.
6. J. Wang, H.H. Wu, D.F. Gao, S. Miao, G.X. Wang and X.H. Bao, *Nano Energy*, 2015, **13**, 387-396.
7. H. Cheng, M.L. Li, C.Y. Su, N. Li and Z.Q. Liu, *Adv. Funct. Mater.*, 2017, **27**, 1701833.
8. G.H. Liu, J.D. Li, J. Fu, G.P. Jiang, G. Lui, D. Luo, Y.P. Deng, J. Zhang, Z.P. Cano, A. Yu, D. Su, Z.Y. Bai, L. Yang and Z.W. Chen, *Adv. Mater.*,2019, **31**, 1970043.
9. I.S. Amiinu, Z.H. Pu, X.B. Liu, K.A. Owusu, H.G.R. Monestel, F.O. Boakye, H.N. Zhang and S.C. Mu, *Adv. Funct. Mater.*, 2017, **27**, 1702300.
10. X.P. Sun, S.X. Sun, S.Q. Gu, Z.F. Liang, J.X. Zhang, Y.Q. Yang, Z. Deng, P. Wei, J. Peng, Y. Xu, C. Fang, Q. Li, J.T. Han, Z. Jiang and Y.H. Huang, *Nano Energy*, 2019, **61**, 245-250.
11. F.L. Meng, H.X. Zhong, D. Bao, J.M. Yan and X.B. Zhang, *J. Am. Chem. Soc.*, 2016, **138**,

10226-10231.

12. L. Yang, X.F. Zeng, D. Wang and D.P. Cao, *Energy Storage Mater.*, 2018, **12**, 277-283.
13. X.E. Liu, M. Park, M.G. Kim, S. Gupta, G. Wu and J. Cho, *Angew. Chem. Int. Ed.*, 2015, **54**, 9654-9658.
14. W.W. Liu, J. Zhang, Z.Y. Bai, G.P. Jiang, M. Li, K. Feng, L. Yang, Y.L. Ding, T.W. Yu, Z.W. Chen and A.P. Yu, *Adv. Funct. Mater.*, 2018, **28**, 1706675.
15. G.B. Chen, J. Zhang, F.X. Wang, L.L. Wang, Z.Q. Liao, E. Zschech, K. Müllen and X.L. Feng, *Chem. Eur. J.*, 2018, **24**, 18413-18418.
16. J. Yin, Y.X. Li, F. Lv, Q.H. Fan, Y.Q. Zhao, Q.L. Zhang, W. Wang, F.Y. Cheng, P.X. Xi and S.J. Guo, *ACS Nano*, 2017, **11**, 2275-2283.
17. P.T. Liu, D.Q. Gao, W. Xiao, L. Ma, K. Sun, P.X. Xi, D.S. Xue and J. Wang, *Adv. Funct. Mater.*, 2018, **28**, 1706928.
18. Q. Liu, Y.B. Wang, L.M. Dai and J.N. Yao, *Adv. Mater.*, 2016, **28**, 3000-3006.
19. X. Zhang, R.R. Liu, Y.P. Zang, G.Q. Liu, G.Z. Wang, Y.X. Zhang, H.M. Zhang and H.J. Zhao, *Chem. Commun.*, 2016, **52**, 5946-5949.
20. J.T. Zhang, Z.H. Zhao, Z.H. Xia and L.M. Dai, *Nat. Nanotechnol.*, 2015, **10**, 444-452.
21. H.B. Yang, J.W. Miao, S.F. Hung, J.Z. Chen, H.B. Tao, X.Z. Wang, L.P. Zhang, R. Chen, J.J. Gao, H.M. Chen, L.M. Dai and B. Liu, *Sci. Adv.*, 2016, **2**, e1501122.
22. Z.Y. Guo, C. Li, W.Y. Li, H. Guo, X.L. Su, P. He, Y.G. Wang and Y.Y. Xia, *J. Mater. Chem. A.*, 2016, **4**, 6282-6289.